

State of Health Estimation for Battery Modules with Parallel-Connected Cells Under Cell-to-Cell Variations

Qinan Zhou^{1,*}, Dyche Anderson², and Jing Sun³

Abstract—State of health (SOH) estimation for lithium-ion battery modules with cells connected in parallel is a challenging problem, especially with cell-to-cell variations. Incremental capacity analysis (ICA) and differential voltage analysis (DVA) are effective at the cell level, but a generalizable method to extend them to module-level SOH estimation remains missing, when only module-level measurements are available. This paper proposes a new method and demonstrates that, with multiple features systematically selected from the module-level ICA and DVA, the module-level SOH can be estimated with high accuracy and confidence in the presence of cell-to-cell variations. First, an information theory-based feature selection algorithm is proposed to find an optimal set of features for module-level SOH estimation. Second, a relevance vector regression (RVR)-based module-level SOH estimation model is proposed to provide both point estimates and three-sigma credible intervals while maintaining model sparsity. With more selected features incorporated, the proposed method achieves better estimation accuracy and higher confidence at the expense of higher model complexity. When applied to a large experimental dataset, the proposed method and the resulting sparse model lead to module-level SOH estimates with a 0.5% root-mean-square error and a 1.5% average three-sigma value. With all the training processes completed offboard, the proposed method has low computational complexity for onboard implementations.

Keywords—Lithium-Ion Battery; State of Health Estimation; Modules with Parallel-Connected Cells; Cell-to-Cell Variation; Feature Selection; Incremental Capacity Analysis

NOMENCLATURE

A	Set of All Features
F, G, H	Random Variable
I	Mutual Information or Conditional Mutual Information
\tilde{I}	Normalized Mutual Information or Normalized Conditional Mutual Information
i, j, l	Index
K	Kernel Function
N	Total Number of Sample Points
Q_c	Charged Capacity
\mathcal{R}	Removed Feature Set
\mathcal{S}	Ranked Selected Feature Set
\mathcal{U}	Set of Features Not Selected Yet
V	Voltage

w	Weight Vector
X	Feature Random Variable
x	Input Vector
Y	Output Random Variable
y	Vector Containing All Outputs in the Dataset
Z	Any Random Variables or Combinations of Random Variables
α	Vector with α_i where α_i^{-1} = Variance of i -th Weight Distribution
β	Scalar where β^{-1} = Variance of Noise Distribution
μ	Mean Vector
Φ	Kernel Matrix
Σ	Covariance Matrix

I. INTRODUCTION

Lithium-ion battery state of health (SOH) estimation with onboard measurements is an active research topic for electrified vehicles [1]. SOH, representing the degradation status of batteries, is critical information for battery management systems [2]. Depending on the applications, SOH may be defined as resistance rising, capacity fading, or their combinations [3], [4]. This paper focuses on capacity fading, and degradation in SOH results in the range reduction of electrified vehicles [4].

While there is a rich set of methodologies and results in the literature for SOH estimation, most of the work reported focuses on the cell level [2], [3], [5], using model-based and data-driven methods. Popular model-based methods include Bayesian filters [6]–[8], sliding-mode observers [9], and least-square techniques [10]. However, given complicated degradation processes, robust and accurate estimation is difficult to achieve with simple phenomenological or physical models using only onboard measurements. On the other hand, data-driven methods have the advantage of not requiring physics-based models. Various data-driven methods include convolutional and recurrent neural networks [11]–[13]. Without insights and structures from physics-based models, however, the effectiveness of these methods solely relies on the comprehensiveness and quality of training data.

One promising middle ground between model-based and data-driven methods is incremental capacity analysis (ICA) [14]–[16]. Peaks in incremental capacity (IC) curves reflect degradation mechanisms inside batteries [17], [18]. Thus, ICA incorporates aging physics without using complicated mechanistic models. The capability to provide physical insights about degradation is the key strength of ICA over deep neural network-based methods and other data-based

¹Qinan Zhou is with the Department of Mechanical Engineering, University of Michigan, Ann Arbor, MI 48103, USA. Email: qinan@umich.edu

²Dyche Anderson is with Research and Advanced Engineering, Ford Motor Company, Dearborn, MI 48121, USA. Email: rander34@ford.com

³Jing Sun is with the Department of Naval Architecture and Marine Engineering, University of Michigan, Ann Arbor, MI 48103, USA. Email: jingsun@umich.edu

*Corresponding Author.

approaches. Furthermore, this method leverages data-driven techniques to correlate physical features (IC peaks) and SOH, and uses the learned model to estimate SOH [19]. ICA has been shown to be effective for different battery chemistries under different temperatures, C rates, and charging ranges [19]. Differential voltage analysis (DVA), a similar method, has also been demonstrated to be effective for cell-level SOH estimation [20].

Battery packs consist of multiple cells in parallel or series for high-energy and high-power applications [21]. In this paper, a battery module refers to a set of battery cells connected in parallel, and the module-level SOH is defined as:

$$\text{SOH} = \frac{Q}{Q_{\text{fresh}}}, \quad (1)$$

where Q and Q_{fresh} are the capacities of a module at its current and fresh state, respectively. While this definition of the module-level SOH has the advantage of directly relating SOH to the module-level capacity, it should be noted that it does not capture cell-to-cell variations within modules. For example, a 95% SOH module can consist of three cells all having 95% cell-level SOHs or three cells with 100%, 95%, and 90% cell-level SOHs, respectively.

For battery modules with cells connected in parallel, inevitable cell-to-cell variations within modules exist in cell capacities, internal resistances, contact resistances, temperatures, etc. [22], [23]. Different papers in the literature have reported contradictory results about the evolution of cell-to-cell variations within modules over time. Take cell-to-cell variations in capacities and internal resistances as examples. [24] and [25] have reported that capacities and internal resistances of individual cells within modules converge due to self-balancing, whereas [22] and [23] have reported diverging results. Thus, unless the research community comes to a solid conclusion about how cell-to-cell variations within modules will evolve, the module-level SOH estimation must be performed under the assumption that cell-to-cell variations exist within battery modules.

For module-level SOH estimation, however, cell-to-cell

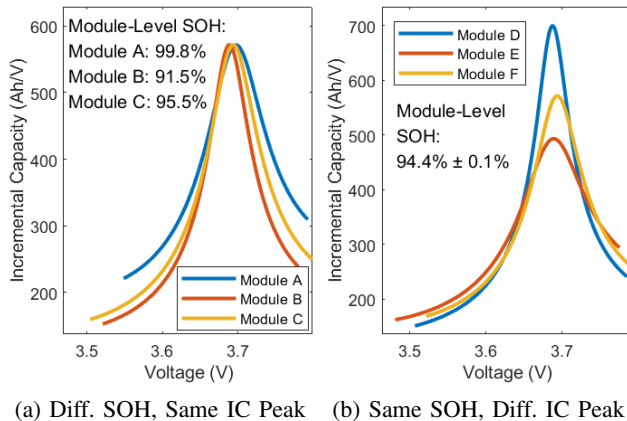


Fig. 1: Example Module-Level IC Curves around an IC Peak in the Presence of Cell-to-Cell Variations

variations within modules hinder ICA- and DVA-based methods [26]. Cell-to-cell variations cause uneven current distribution among individual cells and, thus, distort the module-level IC and DV features [27]. Take IC peak, a feature used for cell-level SOH estimation [14]–[16], [19], as an example. For lithium nickel-manganese-cobalt oxide 622 (NMC622) modules with three cells connected in parallel (208Ah nominal module capacity), experimental data show that the module-level IC peak could be the same for modules with different module-level SOH (Fig. 1a) or different for modules with the same module-level SOH (Fig. 1b) under 86A constant-current charging and room temperature. Thus, the correlation between IC peaks and SOH is obscured by cell-to-cell variations, but these are only phenomenological observations and the insensitivity of these features could disappear when battery chemistries or charging conditions change. For example, IC peaks and distances between two DV inflection points are found robust to cell-to-cell variations in [27] and [28], respectively, for lithium iron phosphate (LFP) modules under their specific conditions. However, for the NMC622 modules discussed above, the IC peak changes significantly due to cell-to-cell variations, while only one DV inflection point exists at the module level. Thus, a generalizable method to find optimal module-level IC and DV features for module-level SOH estimation is still missing.

In this paper, a new and generalizable method, as shown in Fig. 2, is proposed to estimate module-level SOH with high accuracy and confidence in the presence of cell-to-cell variations. Instead of selecting features based on phenomenological observations as in the existing approaches, this paper proposes an algorithm that can find optimal features for module-level SOH estimation. The optimal features can change when situations change, but the proposed algorithm stays the same. Thus, the proposed algorithm is generalizable. Specifically, the contributions of the paper are three-fold:

- First, an information theory-based feature selection algorithm is proposed to find an optimal set of features for module-level SOH estimation. The feature selection process is independent of subsequent learning algorithms. To the best of our knowledge, it is the first application of the information theory-based feature selection to module-level SOH estimation.
- Second, a relevance vector regression (RVR)-based SOH estimation model is developed to not only extract point estimates for SOH but also obtain three-sigma credible intervals. The sparsity of the model is automatically imposed, which leads to low model complexity and makes it suitable for onboard implementations.
- Third, applied to a large dataset of NMC622 modules, the proposed method achieves a good module-level SOH estimation performance (0.5% root-mean-square error (RMSE) and 1.5% average three-sigma value) with a low computational requirement, making it feasible for onboard implementations.

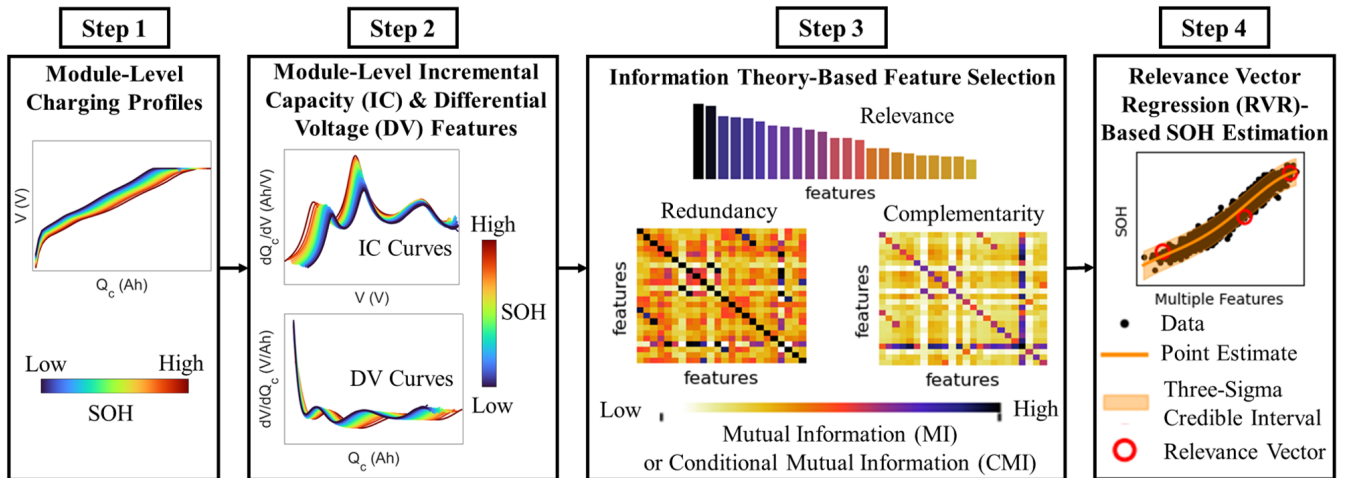


Fig. 2: Overview of Proposed Module-Level State of Health Estimation Method

To elucidate the proposed method in Fig. 2, the paper is organized as follows. Section II summarizes all the IC and DV features related to SOH in general. Section III develops the proposed information theory-based feature selection algorithm. Section IV presents the proposed RVR-based SOH estimation model. Section V discusses the battery datasets used in this study. Section VI demonstrates how to interpret the proposed method using experimental battery cell data. Section VII assesses the performance of the proposed method using experimental battery module data and discusses the onboard computational requirements involved with the implementation of the proposed method. Section VIII summarizes the paper.

II. BATTERY MODULE-LEVEL IC AND DV FEATURES

This section deals with Step 2 of Fig. 2 where all the available features in module-level IC and DV curves are extracted. Given measured module-level charged capacity-voltage (Q_c - V) profiles under constant-current regimes, the module-level IC and DV are defined as $IC = dQ_c/dV$ and $DV = dV/dQ_c$, respectively. In this study, support vector regression is used to fit the measured profiles and, then, module-level IC and DV curves are obtained through analytical derivative calculations to mitigate noise sensitivity caused by numerical derivatives [14]–[16].

The following features, as defined graphically in Fig. 3, can be extracted from the IC and DV curves. For IC features, as shown in Fig. 3a, the x - and y -coordinates of IC peaks and valleys are their locations and heights, respectively. IC peak areas 1, 2, and 3 are the areas from the minimum voltage to the first IC valley location, from the first to the second IC valley locations, and from the second IC valley location to the maximum voltage, respectively [29]. IC peak partial areas can be defined as the area either above a user-defined horizontal cutoff line or within a user-defined symmetric voltage window around a target IC peak [30], as shown in Fig. 3b. Similarly, DV features, as defined in Fig. 3c, include the locations (x -coordinates) and heights (y -coordinates) of

DV peaks and valleys. For charging condition features, temperatures and C rates of constant-current charging regimes affect IC and DV curves. Thus, they are also important features for SOH estimation [19].

Table I summarizes all the available features from ICA, DVA, and charging conditions. Their physical meanings and relations to battery degradation are discussed in the references in Table I. Note that, depending on battery chemistries and charging conditions, some features in Table I might not be available in practice, resulting in different numbers of features for different datasets (as to be seen in Section V).

TABLE I: Summary of Features from ICA, DVA, and Charging Conditions

Feature Category	Acronym	Reference	
IC Peak Height [Ah/V]	IC PH	[17] [18] [31]	
IC Peak Location [V]	IC PL		
DV Valley Height [V/Ah]	DV VH		
DV Valley Location [Ah]	DV VL		
IC Valley Height [Ah/V]	IC VH		
IC Valley Location [V]	IC VL		
DV Peak Height [V/Ah]	DV PH		
DV Peak Location [Ah]	DV PL		
IC Peak Area [Ah]	IC AR		[29]
IC Peak Partial Area [Ah]	IC PA		[30]
Temperature [°C]	-	[19]	
C Rate [C]	-		

III. INFORMATION THEORY-BASED FEATURE SELECTION

The total number of features that can be extracted from ICA, DVA, and charging conditions could be very large. It is necessary to select a subset of features for SOH estimation and avoid the “curse of dimensionality” [32]. This section corresponds to Step 3 of Fig. 2 where an algorithm is proposed to find optimal sets of features for SOH estimation.

Compared to other approaches, the information theory-based feature selection approach is adopted in this work for its excellent capability to capture nonlinear relationships and interactions among multiple features and targets, abundance of feature selection criteria established in the literature, and

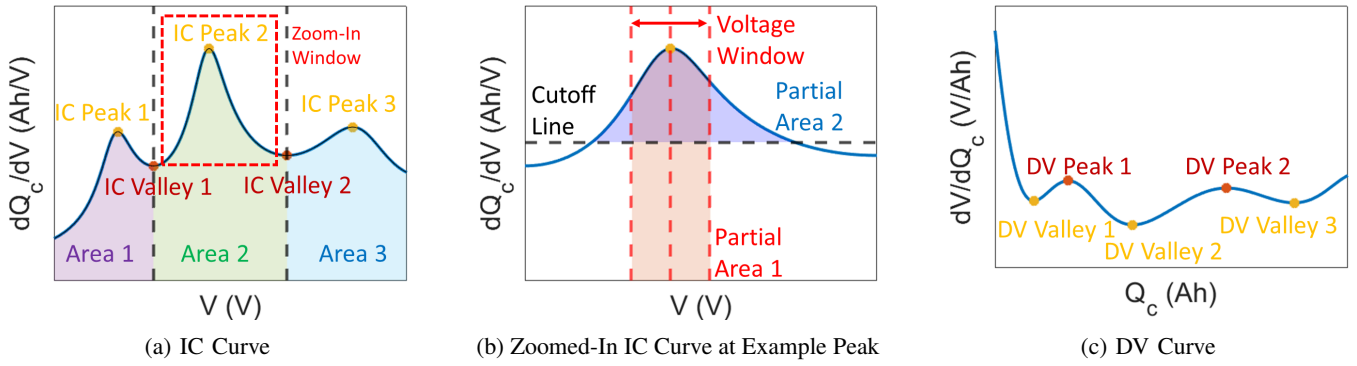


Fig. 3: Definitions of Incremental Capacity (IC) and Differential Voltage (DV) Features

computational efficiency [32]. In the context of module-level SOH estimation, this approach leverages data to infer underlying physical insights in the presence of cell-to-cell variations. Moreover, its results are independent of subsequent SOH estimation algorithms [32], providing the flexibility for adopting different methods in Step 4 of Fig. 2 for the final SOH estimation.

A. Definitions

To present the proposed algorithm, the related concepts and terminologies are defined first. Mutual information (MI) and conditional mutual information (CMI) are two key concepts for information theory-based feature selection [32]. Most generally, they are defined among a mixture of continuous and discrete random variables (RV) using measure theory [33], [34]. Considering three discrete RVs F , G , and H , the MI between F and G is defined as:

$$I(F; G) = \sum_{f \in F} \sum_{g \in G} p(f, g) \log \frac{p(f, g)}{p(f)p(g)}, \quad (2)$$

and the CMI between F and G given H are defined as:

$$I(F; G|H) = \sum_{h \in H} \left\{ p(h) \cdot \sum_{f \in F} \sum_{g \in G} p(f, g|h) \log \frac{p(f, g|h)}{p(f|h)p(g|h)} \right\}, \quad (3)$$

where $p(\cdot)$ is the probability distribution function [35]. If F , G , and H are continuous RVs, summations in these definitions are replaced by integrations [36]. Here, natural logarithms are used. Intuitively, the MI measures the uncertainty reduction of an RV if another RV is known, while the CMI measures the uncertainty reduction of an RV if another RV is known given the third RV [35].

When uncertainty itself varies greatly from RV to RV, MI (uncertainty reduction) and CMI (conditional uncertainty reduction) become ambiguous [37]. Thus, they should be normalized [37]. This paper uses the following normalized MI and CMI [38]:

$$\tilde{I}(F; G) = \frac{I(F; G)}{\min(I(F; F), I(G; G))}, \quad (4)$$

$$\tilde{I}(F; G|H) = \frac{I(F; G|H)}{\min(I(F; F), I(G; G))}. \quad (5)$$

Normalization (4) is chosen to keep the symmetry property of the unnormalized MI [38] and provide a number in $[0, 1]$, similar to a correlation coefficient [37]. Note that Normalization (5) is with respect to $\min(I(F; F), I(G; G))$, instead of $\min(I(F; F|H), I(G; G|H))$. This is a decision made for the feature selection of SOH estimation problems to avoid numerical issues, as to be discussed in Remark 3, Section VI.

B. Feature Selection Algorithm

In general, searching for the globally optimal set of features is NP-hard and heuristic sequential search routines could be used [32]. The widely-used forward search algorithm is adopted in this paper, because of its computational efficiency [39]. It adds new features to a set \mathcal{S} one by one according to a feature selection criterion, which will be discussed later in this subsection. The order in which features are added reflects their relative importance to SOH estimation. Thus, the output \mathcal{S} is a ranked set. The ranking can be used to select a proper subset of \mathcal{S} for SOH monitoring with a relatively simple model. Note that the selected features could be sub-optimal due to the greedy nature of the search algorithm [32].

The pseudo-code for the proposed feature selection algorithm is given in Algorithm 1. Symbols used in Algorithm 1 are defined as: \mathcal{A} – the set of all features, \mathcal{S} – ranked selected feature set, \mathcal{U} – the set of features not selected yet, \mathcal{R} – removed feature set. \mathcal{S} and \mathcal{R} are the outputs of Algorithm 1.

Starting with $\mathcal{S} = \emptyset$, features are added into \mathcal{S} iteratively according to Algorithm 1. At the l -th iteration, given \mathcal{S}_{l-1} and \mathcal{U}_{l-1} resulted from the previous iteration, the algorithm solves the following optimization problem:

$$X_l^* = \operatorname{argmax}_{X \in \mathcal{U}_{l-1}} J(X), \quad (6)$$

where the feature selection criterion $J(X)$ is modified from the joint mutual information criterion [40] and defined as:

$$J(X) = \tilde{I}(X; Y) - \frac{1}{|\mathcal{S}_{l-1}|} \sum_{X_j \in \mathcal{S}_{l-1}} \tilde{I}(X; X_j) + \frac{1}{|\mathcal{S}_{l-1}|} \sum_{X_j \in \mathcal{S}_{l-1}} \tilde{I}(X; X_j|Y), \quad (7)$$

Algorithm 1: Proposed Information Theory-Based Feature Selection Algorithm

Output: ranked selected feature set \mathcal{S} , unranked removed feature set \mathcal{R}

Input: set \mathcal{A} containing all the features, threshold \tilde{I}_{th} for removing completely redundant features

Initialization: $\mathcal{S} \leftarrow \emptyset$ or {pre-selected features}, $\mathcal{R} \leftarrow \emptyset$, $\mathcal{U} \leftarrow \mathcal{A} \setminus \mathcal{S}$

Find completely redundant features to any pre-selected features: $\mathcal{D} \leftarrow \left\{ X \in \mathcal{U} : \tilde{I}(X; X_j) \geq \tilde{I}_{\text{th}}, X_j \in \mathcal{S} \right\}$

$\mathcal{U} \leftarrow \mathcal{U} \setminus \mathcal{D}$, $\mathcal{R} \leftarrow \mathcal{R} \cup \mathcal{D}$

while $|\mathcal{U}| > 0$ **do**

if $|\mathcal{S}| = 0$ **then**

$X^* \leftarrow \operatorname{argmax}_{X \in \mathcal{U}} \tilde{I}(X; Y)$

else

$X^* \leftarrow \operatorname{argmax}_{X \in \mathcal{U}} \left(\tilde{I}(X; Y) - \frac{1}{|\mathcal{S}|} \sum_{X_j \in \mathcal{S}} \tilde{I}(X; X_j) + \frac{1}{|\mathcal{S}|} \sum_{X_j \in \mathcal{S}} \tilde{I}(X; X_j | Y) \right)$

$\mathcal{S} \leftarrow \mathcal{S} \cup \{X^*\}$, $\mathcal{U} \leftarrow \mathcal{U} \setminus \{X^*\}$

 Find completely redundant features to X^* : $\mathcal{D} \leftarrow \left\{ X \in \mathcal{U} : \tilde{I}(X^*; X) \geq \tilde{I}_{\text{th}} \right\}$

$\mathcal{U} \leftarrow \mathcal{U} \setminus \mathcal{D}$, $\mathcal{R} \leftarrow \mathcal{R} \cup \mathcal{D}$

where $|\cdot|$ is the cardinality of a set, $X \in \mathcal{U}_{l-1}$ is a feature not selected yet, $X_j \in \mathcal{S}_{l-1}$ are selected features (j is an index), and Y is the output (i.e., SOH). $J(X)$ contains three terms, namely the relevance $\tilde{I}(X; Y)$, the average redundancy $1/|\mathcal{S}_{l-1}| \cdot \sum_{X_j \in \mathcal{S}_{l-1}} \tilde{I}(X; X_j)$, and the average complementarity $1/|\mathcal{S}_{l-1}| \cdot \sum_{X_j \in \mathcal{S}_{l-1}} \tilde{I}(X; X_j | Y)$. These terms are explained as follows:

- **Relevance:** The relevance of X to Y is defined as the normalized MI between them, i.e., $\tilde{I}(X; Y)$. The higher the relevance is, the more information is shared between X and Y . For cell-level SOH estimation, maximizing the relevance picks up features physically related to SOH. For module-level SOH estimation, features with high relevance are physically related to SOH and have small sensitivity to cell-to-cell variations.
- **Redundancy:** The redundancy between X and X_j is defined as the normalized MI between them, i.e., $\tilde{I}(X; X_j)$. A high redundancy implies that X and X_j have a lot in common, so there is no need to keep both. $\sum_{X_j \in \mathcal{S}_{l-1}} \tilde{I}(X; X_j)$ gives the total redundancy between X and all the selected features in \mathcal{S}_{l-1} . Since this total redundancy grows very fast as the cardinality of \mathcal{S}_{l-1} increases through iterations, the factor $1/|\mathcal{S}_{l-1}|$ is multiplied to bring down the scale [40]. The proposed algorithm minimizes redundancy.
- **Complementarity:** The complementarity captures the “synergy” between two features [41]. Some features could have low relevance to Y but become important in the context of other features. For example, the C rate does not show strong relevance to SOH, because SOH cannot be determined given the C rate alone. However, for example, when IC peaks are chosen, the C rate becomes highly important, as the C rate affects IC peaks [19]. The complementarity between X and X_j is defined as the normalized CMI between them given Y , i.e., $\tilde{I}(X; X_j | Y)$. Similarly, $\sum_{X_j \in \mathcal{S}_{l-1}} \tilde{I}(X; X_j | Y)$ is the total complementarity, while $1/|\mathcal{S}_{l-1}|$ provides the

scaling effect [40]. By maximizing the complementarity, the proposed algorithm leverages the “synergy” between the newly selected feature and those in \mathcal{S}_{l-1} .

Thus, for module-level SOH estimation, at each iteration, the proposed algorithm selects the feature based on whether it provides the best trade-off among relevance, redundancy, and complementarity, not on how much it is distorted by cell-to-cell variations. Optimization (6) is performed until $|\mathcal{U}| = 0$.

Remark 1. (On Non-Empty Initialization) \mathcal{S} can also be initialized to contain some pre-selected features based on available physical knowledge. Note that these pre-selected features can be unranked or ranked. For this study, \mathcal{S} is initialized as an empty set to let data speak for themselves.

Remark 2. (On Removing Features) For SOH estimation problems, normalized CMI could be high for both complementary and completely redundant features, causing the latter to be selected. Thus, the feature removal step in Algorithm 1 is necessary. Specifically, at one iteration, if X^* is selected by solving Optimization (6), then the proposed algorithm removes all the features $X \in \mathcal{U}$ whose redundancies $\tilde{I}(X^*; X)$ are above a user-defined threshold \tilde{I}_{th} , i.e., removes the set $\mathcal{D} = \left\{ X \in \mathcal{U} : \tilde{I}(X^*; X) \geq \tilde{I}_{\text{th}} \right\}$ from \mathcal{U} . Thus, these features will not be considered in the next iteration.

C. MI/CMI Estimation and Data Standardization

The proposed algorithm relies on MI and CMI whose definitions involve probability distributions of RVs. However, these distributions are not known in practice. Thus, MI and CMI must be estimated using data.

To have consistent estimation results, this paper uses the k -nearest neighbor (k NN) CMI estimator [34] to calculate both MI and CMI. Consider sample $\left\{ (f_i, g_i, h_i)^T \right\}_{i=1}^N$ from RVs $(F, G, H)^T$ where N is the number of sample points and i is an index. For any sample point $(f_i, g_i, h_i)^T$, one can first define its k -nearest neighbor based on l_∞ -norm distance and denote the corresponding l_∞ -norm distance as $\frac{1}{2}d_{k,i}$. Note

that k is a tuning hyperparameter for the estimator and its proper value is related to the number of data [36]. Next, one can count the number of sample points within different windows:

$$n_{Z,i} = \left| \left\{ z_j : \|z_i - z_j\|_\infty \leq \frac{1}{2}d_{k,i}, i \neq j \right\} \right|, \quad (8)$$

where Z can be any RVs or combinations of RVs (e.g., $(F, H)^T$, $(G, H)^T$, H , etc.), and z can be any sample points from these RVs or combinations of RVs (e.g., $(f, h)^T$, $(g, h)^T$, h , etc.). Finally, by repeating the same process for all the data, the estimator [34] computes the CMI estimates $\hat{I}(F; G|H)$ as:

$$\xi_i = \psi(\tilde{k}_i) - \psi(n_{FH,i}) - \psi(n_{GH,i}) + \psi(n_{H,i}), \quad (9)$$

$$\hat{I}(F; G|H) = \max \left\{ \frac{1}{N} \sum_{i=1}^N \xi_i, 0 \right\}, \quad (10)$$

where \tilde{k}_i is calculated using Equation (8) with Z and z defined as $(F, G, H)^T$ and $(f, g, h)^T$, $\psi(\cdot)$ is the digamma function that satisfies $\psi(x+1) = \psi(x) + 1/x$, $\psi(1) = -C$, and C is the Euler-Mascheroni constant [36].

To estimate MI $\hat{I}(F; G)$, one can still use Equations (9) and (10) by setting H to be an artificially generated white Gaussian noise with a mean of 0 and variance of 1. The white Gaussian noise is generated such that it is independent of F , G , and $(F, G)^T$ jointly. Thus, based on Definitions (2) and (3),

$$\hat{I}(F; G) = \hat{I}(F; G|\text{White Gaussian Noise}). \quad (11)$$

When F , G , and H have different orders of magnitudes (as in the case of IC and DV features), the use of l_∞ -norm in MI and CMI estimation causes numerical problems. A common solution given in the literature is to standardize all the sample points first using:

$$z_i^{(s)} = \frac{z_i - \text{mean}(\{z_i\}_{i=1}^N)}{\text{std}(\{z_i\}_{i=1}^N)} \quad (12)$$

for sample $\{z_i\}_{i=1}^N$ from any RV Z , where $\text{mean}(\cdot)$ and $\text{std}(\cdot)$ are the mean and standard deviation of sample points, respectively [42].

IV. RELEVANCE VECTOR REGRESSION

With the optimal set of features found, the next step is to build a module-level SOH estimation model. This section corresponds to Step 4 of Fig. 2 where the proposed algorithm trains a sparse probabilistic model and estimates module-level SOH as distributions with point estimates and three-sigma credible intervals.

Relevance vector regression (RVR) is a sparse regression technique and the Bayesian counterpart to non-Bayesian support vector regression [43]. RVR is chosen in this work over other regression techniques, because it has the following advantages. First, trained models can be updated based on future data using sequential Bayesian learning [43]. Second,

when making predictions, instead of seeking to have accurately trained model parameters, the RVR integrates over all these unknown parameters, which improves predictive performance and increases robustness [43]. Third, the RVR automatically prefers simple but sufficiently accurate models over complicated models to explain the data [44]. Fourth, kernels in RVR do not need to satisfy Mercer's conditions, allowing higher design freedom [45].

A. Regression Algorithm

This paper uses the original RVR algorithm [46], with customizations in the initialization, kernel choice, hyperparameter values, and stopping conditions to fit the needs of SOH estimation problems. The pseudo-code for training the RVR model is given in Algorithm 2.

Assume independent and identically distributed (I.I.D.) data $\{(\mathbf{x}_i, y_i)\}_{i=1}^N$ where $\mathbf{x} \in \mathbb{R}^{N_f}$ are features, N_f is the number of features, $y \in \mathbb{R}$ is the output (i.e., SOH), i is an index, and N is the number of data. Then, an output y and an input \mathbf{x} can be related by:

$$y = \left(w_0 + \sum_{i=1}^N w_i K(\mathbf{x}, \mathbf{x}_i) \right) + \eta, \quad (13)$$

where \mathbf{x}_i are the input data, w_i and w_0 are weights and offset to be learned, η is the noise in the process which is assumed to be a white Gaussian noise with an unknown variance β^{-1} to be learned, and $K(\cdot, \cdot)$ is a user-defined kernel [46]. This paper uses the radial basis function for the kernel, i.e.,

$$K(\mathbf{x}, \mathbf{x}') = \exp(-\rho \|\mathbf{x} - \mathbf{x}'\|_2^2), \quad (14)$$

where $\|\mathbf{x} - \mathbf{x}'\|_2$ is the Euclidean norm of $\mathbf{x} - \mathbf{x}'$ and ρ is a tunable hyperparameter.

The first step in the RVR is to choose prior distributions [46]. Priors are required for any unknowns one wants to learn and add regularization effects into the training process [47]. The priors for RVR are:

$$p(\mathbf{w}|\boldsymbol{\alpha}) = \prod_{i=0}^N \mathcal{N}(w_i|0, \alpha_i^{-1}), \quad (15)$$

$$p(\boldsymbol{\alpha}) = \prod_{i=0}^N \Gamma(\alpha_i|a, b), \quad (16)$$

$$p(\beta) = \Gamma(\beta|c, d), \quad (17)$$

where $p(\cdot)$ is the probability distribution function, $\mathbf{w} = [w_0 \dots w_N]^T \in \mathbb{R}^{N+1}$ are unknown offset and weights, $\boldsymbol{\alpha} = [\alpha_0 \dots \alpha_N]^T \in \mathbb{R}^{N+1}$ are unknown reciprocals of variances for offset and weights, $\mathcal{N}(\cdot|\cdot, \cdot)$ and $\Gamma(\cdot|\cdot, \cdot)$ are the Gaussian and Gamma distributions respectively, and a , b , c , d are small numbers so that $p(\boldsymbol{\alpha})$ and $p(\beta)$ are flat noninformative priors that do not provide any information to the learning algorithm and, thus, allow the data to speak for themselves [47]. Following [46], this paper chooses $a \rightarrow 0$, $b \rightarrow 0$, $c \rightarrow 0$, $d \rightarrow 0$. Priors in Equations (15) and (16) achieve model sparsity, because these two priors together make the unconditional prior $p(\mathbf{w})$ a student's t distribution [46], a type of very sparse prior distributions [48].

Algorithm 2: Training of the Proposed Relevance Vector Regression (RVR)-Based SOH Estimation Model

Output: relevance vectors $\{\mathbf{rv}_j\}_{j=1}^{N_{rv}}$, reciprocals of variances for offset and weights α_{MP} , noise variance β_{MP}^{-1} , trained/pruned Σ , trained/pruned μ , a boolean variable o about whether offset is used

Input: standardized data $\{(\mathbf{x}_i, y_i)\}_{i=1}^N$, kernel function $K(\cdot, \cdot)$

Initialization: α with $\alpha_i \leftarrow \frac{1}{(N+1)^2}, i = 0, \dots, N$, α^{old} with $\alpha_i^{old} \leftarrow \alpha_i, \beta^{-1} \leftarrow (0.1 \cdot \text{std}(\{y_i\}_{i=1}^N))^2$, a set $\mathcal{E} \leftarrow \{e_0, \mathbf{x}_1, \dots, \mathbf{x}_N\}$ (e_0 serves as a placeholder for offset and can be initialized as anything), maximum number of iterations N_{iter} , threshold α_{th} (a large number), tolerance tol , a small number ε , $\mathbf{y} = [y_1 \dots y_N]^T$, $\Phi \leftarrow [\phi(\mathbf{x}_1) \dots \phi(\mathbf{x}_N)]^T \in \mathbb{R}^{N \times (N+1)}$ where $\phi(\mathbf{x}_i) \leftarrow [1 \ K(\mathbf{x}_i, \mathbf{x}_1) \dots K(\mathbf{x}_i, \mathbf{x}_N)]^T, \forall i = 1, \dots, N$

for $k = 1, \dots, N_{iter}$ **do**

$\mathbf{A} \leftarrow \text{diag}(\alpha), \Sigma \leftarrow \text{Equation (21)}, \mu \leftarrow \text{Equation (22)}$

Update α with all the components $\alpha_i \leftarrow \text{Equation (31)}, \beta^{-1} \leftarrow \text{Equation (26)}$

Find indices that need to be kept: $\{i\}^{keep} \leftarrow \{i | \alpha_i < \alpha_{th}\}$

Prune: $\alpha \leftarrow \alpha[\{i\}^{keep}], \alpha^{old} \leftarrow \alpha^{old}[\{i\}^{keep}], \Sigma \leftarrow \Sigma[\{i\}^{keep}, \{i\}^{keep}], \mu \leftarrow \mu[\{i\}^{keep}], \Phi \leftarrow \Phi[:, \{i\}^{keep}],$
 $\mathcal{E} \leftarrow \mathcal{E} \setminus \{i\}^{keep}$

if $\|\alpha - \alpha^{old}\|_\infty \leq tol$ **and** $k > 1$ **then**

└ break

$\alpha^{old} \leftarrow \alpha$

$\alpha_{MP} \leftarrow \alpha, \beta_{MP}^{-1} \leftarrow \beta^{-1}$

$\{\mathbf{rv}_j\}_{j=1}^{N_{rv}} \leftarrow \begin{cases} \mathcal{E}, & \text{if } e_0 \notin \mathcal{E}, \text{ i.e., the offset is not used} \\ \mathcal{E} \setminus \{e_0\}, & \text{otherwise} \end{cases}, o \leftarrow \begin{cases} \text{False, if the offset is not used} \\ \text{True, otherwise} \end{cases}$

/* ":" means all the rows in matrix Φ */

The next step is to choose a likelihood distribution for the given data [46]. Based on the assumptions of I.I.D. sample points and white Gaussian noises in the process, the likelihood for RVR is:

$$p(\mathbf{y}|\mathbf{w}, \beta) = \mathcal{N}(\mathbf{y}|\Phi\mathbf{w}, \beta^{-1}\mathbf{I}), \quad (18)$$

where $\mathbf{y} = [y_1 \dots y_N]^T$ are outputs, $\Phi = [\phi(\mathbf{x}_1) \dots \phi(\mathbf{x}_N)]^T \in \mathbb{R}^{N \times (N+1)}$ is the kernel matrix, $\phi(\mathbf{x}_i) = [1 \ K(\mathbf{x}_i, \mathbf{x}_1) \dots K(\mathbf{x}_i, \mathbf{x}_N)]^T$ is a vector that contains kernel functions, and \mathbf{I} is the identity matrix.

With priors and likelihood defined, the most fundamental step in Bayesian learning is to compute and update the posterior distribution. Posterior can be computed analytically if a pair of conjugate prior and likelihood is used or approximated using various established methods [47]. For the RVR [46], the posterior is:

$$p(\mathbf{w}, \alpha, \beta|\mathbf{y}) = p(\mathbf{w}|\mathbf{y}, \alpha, \beta) p(\alpha, \beta|\mathbf{y}), \quad (19)$$

where $p(\mathbf{w}|\mathbf{y}, \alpha, \beta)$ can be found analytically because of the conjugate pair chosen, i.e.,

$$p(\mathbf{w}|\mathbf{y}, \alpha, \beta) = \mathcal{N}(\mathbf{w}|\mu, \Sigma), \quad (20)$$

where one defines a diagonal matrix $\mathbf{A} = \text{diag}(\alpha)$ and

$$\Sigma = (\beta\Phi^T\Phi + \mathbf{A})^{-1}, \quad (21)$$

$$\mu = \beta\Sigma\Phi^T\mathbf{y}. \quad (22)$$

$p(\alpha, \beta|\mathbf{y})$ cannot be directly evaluated, but can be approximated. When performing prediction, the effects of $p(\alpha, \beta|\mathbf{y})$ can be approximated well by $\delta(\alpha_{MP}, \beta_{MP})$ where $\delta(\cdot, \cdot)$ is

the delta function and α_{MP} and β_{MP} can be found by solving the Type-II maximum likelihood [46]. Specifically, because $p(\alpha)$ and $p(\beta)$ are noninformative priors by construction, the final formulation for the Type-II maximum likelihood problem is:

$$\alpha_{MP}, \beta_{MP} = \underset{\alpha, \beta}{\text{argmax}} p(\mathbf{y}|\alpha, \beta), \quad (23)$$

$$p(\mathbf{y}|\alpha, \beta) = \mathcal{N}(\mathbf{y}|\mathbf{0}, \beta^{-1}\mathbf{I} + \Phi\mathbf{A}^{-1}\Phi^T), \quad (24)$$

where $\mathbf{0}$ is a vector with all components equal to 0. Thus, the iterative update laws for α and β^{-1} are:

$$\alpha_i = \frac{\gamma_i}{\mu_i^2}, \quad \gamma_i = 1 - \alpha_i^{old}\Sigma_{ii}, \quad (25)$$

$$\beta^{-1} = \frac{\|\mathbf{y} - \Phi\mu\|_2^2}{N - \sum_i \gamma_i}, \quad (26)$$

where Σ_{ii} and μ_i are the i -th diagonal component of matrix Σ and the i -th component of vector μ in Equations (21) and (22) respectively, and \sum in the denominator of Equation (26) is the summation operator.

Note that, as iterations progress, most of the α_i approach ∞ , which makes their corresponding weights w_i have distributions with zero mean and zero variance. These w_i and the corresponding components of $\Sigma, \mu, \Phi, \alpha$, and α^{old} need to be deleted from iterations [46]. The \mathbf{x}_i corresponding to the remaining w_i with nonzero variances are the relevance vectors. This process is called the automatic relevance determination [49].

When predicting outputs, the key strength of Bayesian learning is the integration over unknown parameters. In RVR

[46], given a new input \mathbf{x} , the distribution of estimated output y is:

$$p(y|\mathbf{y}, \boldsymbol{\alpha}_{\text{MP}}, \beta_{\text{MP}}) = \int p(y|\mathbf{w}, \beta_{\text{MP}}) p(\mathbf{w}|\mathbf{y}, \boldsymbol{\alpha}_{\text{MP}}, \beta_{\text{MP}}) d\mathbf{w}. \quad (27)$$

This integral has the analytical solution:

$$p(y|\mathbf{y}, \boldsymbol{\alpha}_{\text{MP}}, \beta_{\text{MP}}) = \mathcal{N}(y|t, \sigma^2), \quad (28)$$

$$t = \boldsymbol{\mu}^T \tilde{\boldsymbol{\phi}}(\mathbf{x}), \quad (29)$$

$$\sigma^2 = \beta_{\text{MP}}^{-1} + \tilde{\boldsymbol{\phi}}(\mathbf{x})^T \boldsymbol{\Sigma} \tilde{\boldsymbol{\phi}}(\mathbf{x}), \quad (30)$$

where $\tilde{\boldsymbol{\phi}}(\mathbf{x}) = [1 \ K(\mathbf{x}, \mathbf{rv}_1) \ \dots \ K(\mathbf{x}, \mathbf{rv}_{N_{\text{rv}}})]^T$ if the offset is used and $\tilde{\boldsymbol{\phi}}(\mathbf{x}) = [K(\mathbf{x}, \mathbf{rv}_1) \ \dots \ K(\mathbf{x}, \mathbf{rv}_{N_{\text{rv}}})]^T$ otherwise, $\mathbf{rv}_j, j = 1, \dots, N_{\text{rv}}$ are the relevance vectors found, N_{rv} is the total number of relevance vectors, and the pruned $\boldsymbol{\Sigma}$ and $\boldsymbol{\mu}$ only contain components corresponding to these relevance vectors after training. With estimate distributions found, this paper uses Equation (29) as the point estimate and extracts the three-sigma credible interval from Equation (30), i.e., $(t - 3\sigma, t + 3\sigma)$.

Five customizations are made in this study to implement the RVR proposed by [46]. First, following the implementations in sklearn-RVM [45], this paper initializes all the α_i to be $1/(N+1)^2$ and β^{-1} to be $(0.1 \cdot \text{std}(\{y_i\}_{i=1}^N))^2$. Second, during the iterative process, this paper performs the aforementioned deletion when $\alpha_i \geq \alpha_{\text{th}}$ where α_{th} is a very large number (e.g., 10^9). Third, this paper stops the iterative process when either the maximum number of iterations N_{iter} is reached or $\|\boldsymbol{\alpha} - \boldsymbol{\alpha}^{\text{old}}\|_{\infty} \leq \text{tol}$ where $\|\cdot\|_{\infty}$ is the l_{∞} -norm and tol is a tunable tolerance. Fourth, to help $\boldsymbol{\Sigma}$ and $\boldsymbol{\mu}$ stay well-conditioned during iterations and make Optimization (23) converge faster, the data $\{(\mathbf{x}_i, y_i)\}_{i=1}^N$ are standardized using Equation (12) before running Algorithm 2. Fifth, to prevent α_i in Equation (25) from becoming very small in practice and slow down the convergence, based on the sklearn-RVM [45], this paper modifies the iterative update law in Equation (25) as:

$$\alpha_i = \frac{\max\{\gamma_i, \varepsilon\}}{\mu_i^2}, \quad \gamma_i = 1 - \alpha_i^{\text{old}} \Sigma_{ii} \quad (31)$$

where ε is a very small number (e.g., 10^{-8}).

V. BATTERY DATASETS

The proposed method in Fig. 2 will be demonstrated and validated using experimental datasets. First, the public Oxford lithium cobalt oxide (LCO) cell dataset [50] (downloading website: [51]) is used to illustrate related concepts and interpret results from the proposed method. The detailed description can be found in [50]. Then, a proprietary lithium nickel-manganese-cobalt oxide 622 (NMC622) module dataset is used to evaluate the performance of the proposed method for module-level SOH estimation under cell-to-cell variations. The existence of cell-to-cell variation within modules and their impacts on IC curves are illustrated in Fig. 1. The entire battery pack containing 96 modules in series is cycled under the charging profiles consisting of two consecutive constant-current regimes with 86A and

64.5A pack-level currents, respectively, and one subsequent constant-voltage regime. Only the first constant-current segment is used for this study, as this segment contains all the IC and DV features for this dataset. The actual data used by the proposed method have a 0.033Hz sampling rate, i.e., 1 measurement per 30 seconds. When the entire pack is charged, passive balancing is used for 96 serially connected modules. The balancing current is very small compared to the module-level current, thus its impact on IC and DV curves is negligible, and the issue discussed in [52] is avoided. Within each module, 3 parallelly connected cells have self-balancing effects and do not involve active or passive balancing.

TABLE II: Key Attributes of Battery Datasets

Type	Attributes
Cell	Chemistry: LCO Cell Nominal Capacity: 0.74Ah No. of Cells: 8 No. of Features: 24 No. of Cycles: 398 Cell-Level SOH Range: 100% - 88%, where all the IC and DV features exist
Module	Chemistry: NMC622 Module Nominal Capacity: 208Ah Module Configuration: 3 cells in parallel No. of Modules: 96 No. of Features: 6 No. of Cycles: 81216 Module-Level SOH Range: 100% - 86%

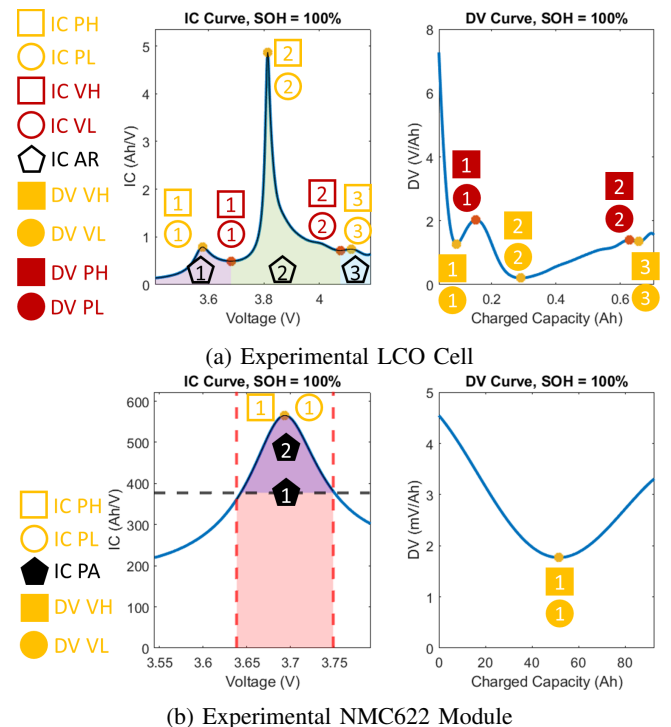


Fig. 4: Example IC and DV Curves and Related Features for Two Datasets

Table II summarizes the key attributes of these two datasets, while Fig. 4 shows their example IC and DV curves and related features. Note that, for ease of discussion, the

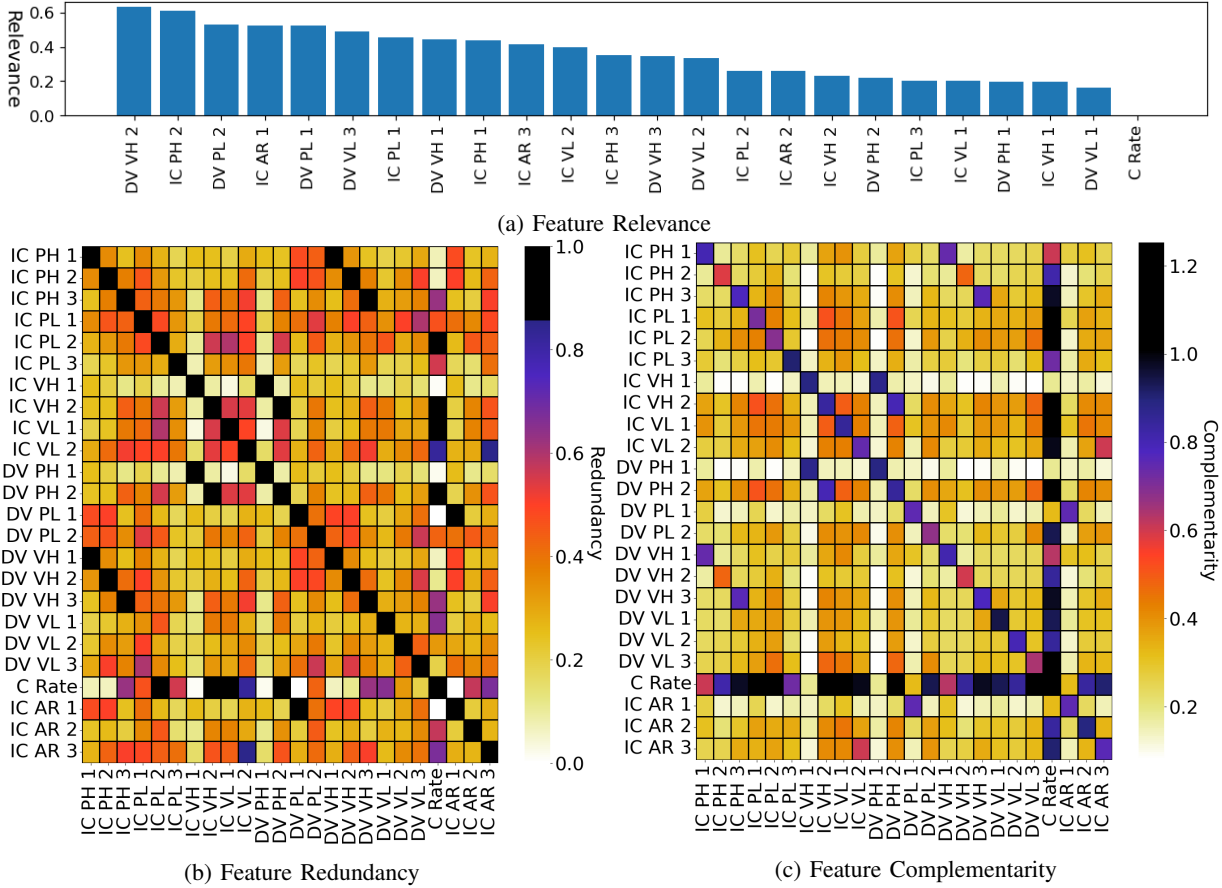


Fig. 5: Feature Relevance, Redundancy, and Complementarity for Cell-Level SOH Estimation under Different C Rates

acronyms in Table I and indices labeled in Fig. 4 will be used together to refer to different features. For example, the left IC peak height in Fig. 4a is denoted as IC PH 1.

VI. INTERPRETATION OF THE PROPOSED METHOD USING CELL DATA

The cell-level SOH estimation is discussed first, because the cell dataset contains a lot more features and charging conditions than the proprietary module dataset, making the cell dataset more suitable to demonstrate the full capability of the proposed feature selection algorithm. Note that the proposed method can be applied to both cell-level and module-level SOH estimations. Nonetheless, as to be seen in Sections VI and VII, the selected optimal sets of features and resulting RVR models are different for cell-level and module-level SOH estimations, as the situations and conditions change.

The Oxford cell dataset is split into 80% training and 20% testing sets. The training data are used for performing the feature selection and building the RVR-based SOH estimation model, while testing data are used to evaluate the performance. For running the proposed method, as discussed in Sections III-C and IV, SOH values and all the features are standardized based on the corresponding means and standard deviations of the training set using Equation (12). Then, for result discussions, all these standardized quantities are converted back for physical interpretations.

Fig. 5 shows the relevance, redundancy, and complementarity among all the features. One can observe from Fig. 5a that: (1) DV VH 2 has the highest relevance to SOH and it will be the first feature selected by the algorithm when there is no pre-selected feature; (2) C rate has no relevance to SOH, because physically a battery can be at any SOH when charged at a given C rate.

The black color in Fig. 5b represents redundancy values above the threshold \tilde{I}_{th} . The darker the color is, the higher the redundancy is. From Fig. 5b, one can observe the following. First, IC peak/valley heights and DV valley/peak heights are completely redundant, because $IC = 1/DV$. Second, DV PL 1 and IC AR 1 are completely redundant. From the definition, $IC\ AR\ 1 = \int_{V_{min}}^{V_{IC\ valley\ 1}} \frac{dQ_c}{dV} dV = Q_{c,IC\ valley\ 1} - 0 = DV\ PL\ 1$, where Q_c is the charged capacity, V is the voltage. Third, the C Rate is completely redundant to IC PL 2, IC VH 2, IC VL 1, and DV PH 2. Note that this observation is only applicable to this dataset.

Based on Fig. 5c, complementarity between the C rate and most of the IC and DV features is high, because the values of most features have C rate dependency. Thus, in the case where these features are selected, the C rate will be selected because of the complementarity in Equation (7), unless the C rate is completely redundant to the associated feature. Note that, from Fig. 5c, completely redundant features also have

TABLE III: Feature Selection Results for Cell-Level SOH Estimation of LCO Cells under Different C Rates

Ranked Selected Feature Set, S	{ DV VH 2, C Rate, DV VL 3, DV VH 1, DV PL 2, IC PL 1, IC AR 3, DV PL 1, IC VL 2, IC PH 3, DV VL 2, IC AR 2, IC PL 3, DV VL 1, DV PH 1 }
Unranked Removed Feature Set, \mathcal{R}	{ IC PH 1, IC PH 2, IC PL 2, IC VH 1, IC VH 2, IC VL 1, DV PH 2, DV VH 3, IC AR 1 }

high CMI, but they will not be selected because of the feature removal process in Algorithm 1.

Remark 3. (On Normalization of CMI) The denominator of Normalization (5) is $\min(I(F; F), I(G; G))$, instead of $\min(I(F; F|H), I(G; G|H))$, because the normalized value using $\min(I(F; F|H), I(G; G|H))$ is less interpretable in some situations of this case study. For example, consider the normalized CMI $\tilde{I}(\text{IC PH 1}; \text{DV VH 1}|\text{SOH})$. Given $\tilde{I}(\text{IC PH 1}; \text{SOH}) = 0.4364 > 0$, logically the CMI should be a lot less than 1, because the uncertainty of IC PH 1 has been already reduced by knowing SOH. Definition (5) gives $\text{CMI} = 0.7415$, but normalization with respect to $\min(I(F; F|H), I(G; G|H))$ gives $\text{CMI} = 0.9242 \approx 1$.

Remark 4. (On Values of Normalized CMI) Note that, because of the estimation inaccuracy of the used CMI estimator, the normalized CMI could occasionally become a little above 1, as shown in Fig. 5c.

With relevance, redundancy, and complementarity obtained above, Algorithm 1 outputs the ranked selected feature set and unranked removed feature set, as summarized in Table III. Note that the DV VH 2 (equivalently, IC PH 2) and C rate are the top two ranked features, which matches the physical knowledge from [19].

These top two ranked features are used to build a cell-level SOH estimation model. Based on Table IV, the proposed model has a low computational complexity (small number of relevance vectors, \mathbf{rv}_j) and high estimation accuracy (low test root-mean-square error, RMSE). Fig. 6 shows the trained model under different C rates and the three-sigma (99.7%) credible intervals for different SOHs. Table IV also summarizes the average three-sigma values.

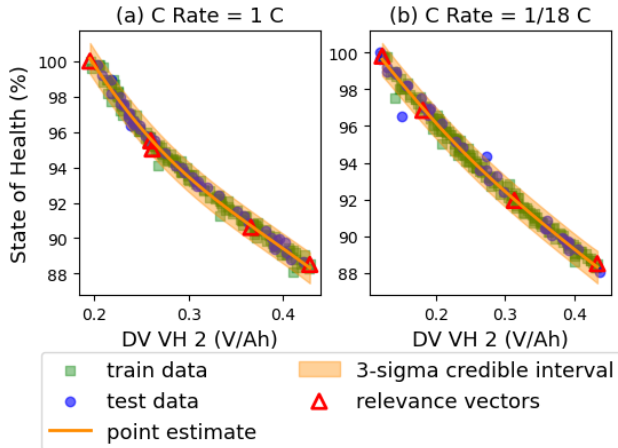


Fig. 6: Cell-Level SOH Estimation Model Using Two Features

TABLE IV: Cell-Level SOH Estimation Results

Train RMSE	Number of \mathbf{rv}_j	Average Three-Sigma Values	Test RMSE
0.27% SOH	9	0.84% SOH	0.33% SOH

VII. MODULE-LEVEL SOH ESTIMATION RESULTS UNDER CELL-TO-CELL VARIATIONS

This section presents the results of module-level SOH estimation in the presence of cell-to-cell variations, using the experimental NMC622 module data to demonstrate real-world performance. Furthermore, this section investigates the onboard computational footprint of the proposed method.

A. Module-Level SOH Estimation Performance

4060 sample points are randomly selected from the large dataset for both feature selection and RVR model development, while the remaining 77156 sample points are used for testing the performance. Results from the two-sample Kolmogorov-Smirnov test [53], Anderson-Darling test [54], and Cramér-von Mises criterion [55] all indicate that the randomly selected 4060 sample points have the same distribution as the original dataset. To apply the proposed method, due to reasons discussed in Sections III-C and IV, SOH values and all the features of the entire dataset are standardized based on the corresponding means and standard deviations of the training set using Equation (12). Then, all these standardized quantities are converted back, in result discussions, for physical interpretations.

TABLE V: Feature Selection Results for Module-Level SOH Estimation in the Presence of Cell-to-Cell Variations

Ranked Selected Feature Set, S	IC PA 1 IC PA 2 IC PH 1 DV VL 1 IC PL 1
Unranked Removed Feature Set, \mathcal{R}	DV VH 1

The proposed Algorithm 1 finds the optimal set of features for module-level SOH estimation in the presence of cell-to-cell variations. Table V summarizes the module-level feature selection results. IC PA 1 is the top-ranked feature, which is not only related to SOH but also the most insensitive to cell-to-cell variations. Other features are selected, according to the trade-off they provide among relevance, redundancy, and complementarity, instead of how insensitive they are to cell-to-cell variations. Referring back to the issue shown in Fig. 1, even though IC PH 1 is significantly distorted by cell-to-cell variations, the proposed method finds that IC PH 1 provides the best trade-off among relevance, redundancy, and

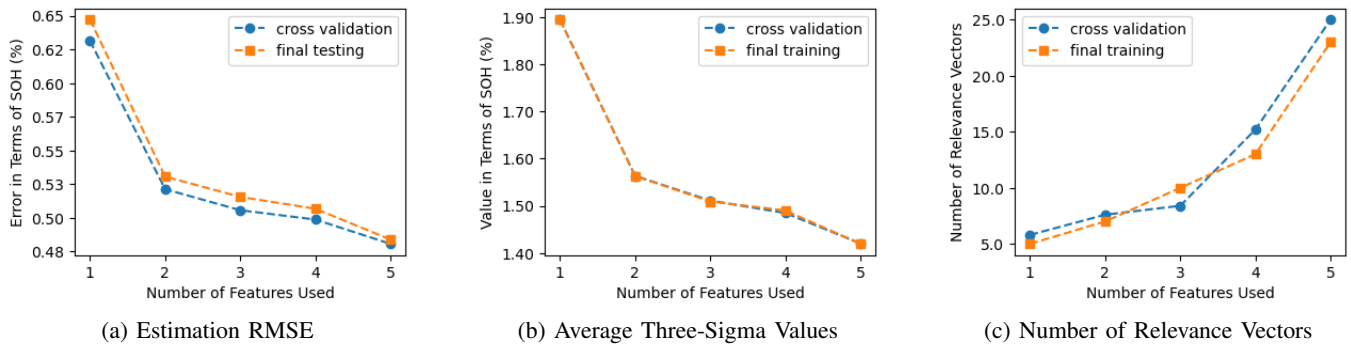


Fig. 7: Module-Level SOH Estimation Performance under Different Number of Features Used

complementarity, once IC PA 1 and IC PA 2 are selected. Thus, instead of using IC PH 1 as a sole feature for SOH estimation, the proposed algorithm recommends IC PH 1 to be used together with IC PA 1 and IC PA 2 to provide optimal estimation performance for this dataset.

With all the available features ranked, the SOH estimation model is trained using Algorithm 2. The proper number of features for the SOH estimation model can be determined by applying five-fold cross-validation to the training data. The average validation RMSE, the average number of relevance vectors, and the average three-sigma values from the five-fold cross-validation are used to evaluate the estimation accuracy, model complexity, and estimation uncertainty, respectively.

The final SOH estimation model is trained using all the training data, and Table VI summarizes the final testing RMSE, number of relevance vectors, and average three-sigma values when different numbers of features are used. Note that IC PH 1 is the feature commonly used in the literature [14]–[16], [19] and, thus, Model 0 in Table VI will be used as the baseline for discussion. However, IC PH 1 is only ranked in third place by the feature selection algorithm. Based on Table VI, even the SOH estimation model using only one feature selected by the proposed algorithm (i.e., Model 1) can significantly outperform the conventional SOH estimation model (i.e., Model 0). From another perspective, these results also exemplify the significant extent to which cell-to-cell variations can impact SOH estimation. The most robust feature against cell-to-cell variation in this dataset (i.e., IC PA 1) can achieve roughly 1/2 of both the test RMSE and average three-sigma value that a sensitive feature (i.e., IC PH 1) can achieve.

To reflect the trade-off between estimation performance and model complexity, Fig. 7 shows how the RMSE, number of relevance vectors, and average three-sigma values vary with the number of features used in the SOH estimation model for cross-validation and testing. Fig. 8 shows the absolute estimation error distribution for all the testing data when only two features are used. Based on Table VI, Fig. 7, and Fig. 8, several important conclusions could be made:

- Leveraging properly selected multiple features indeed improves module-level SOH estimation accuracy and reduces estimation uncertainty.
- Better performance for module-level SOH estimation

can be achieved at the expense of higher model complexity. Using only two or three features provides a good trade-off between estimation performance and model complexity.

- Module-level SOH can indeed be estimated with high accuracy and confidence in the presence of cell-to-cell variations. Note that the proposed method does not use any information about cell-to-cell variations explicitly.

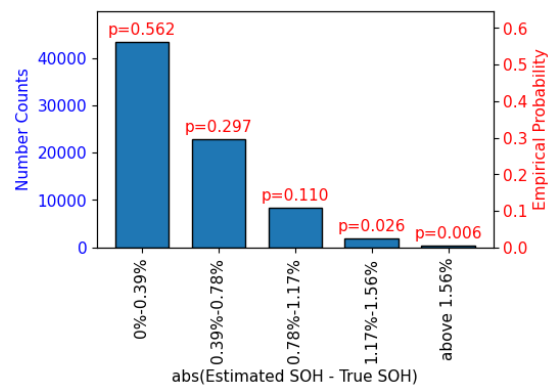


Fig. 8: Testing Absolute Error Distribution from Two-Feature SOH Estimation Model

Remark 5. For the proposed SOH estimation method, charging ranges do not necessarily have to be full but have to be long enough to include the selected features. Since the SOH estimation, unlike the state of charge estimation, does not need to be performed continuously for all operations, a condition can be included in the algorithm so that SOH estimation is only performed when there are sufficient data points and bypassed when charging ranges are short.

B. Onboard Implementation of the Proposed Method

The proposed method in Fig. 2 has both offboard and onboard computations involved. The proposed feature selection algorithm in Step 3 of Fig. 2 is performed completely offboard to find the optimal set of features for module-level SOH estimation. The onboard computation involves: (1) extracting the values of these selected features from module-level IC and DV curves and (2) estimating SOH according to the RVR model developed in Step 4 of Fig. 2.

TABLE VI: Module-Level SOH Estimation Results for Modules with Cell-to-Cell Variations under Different Number of Features Used

Model Name	Number of Features	Selected Features	Number of Relevance Vectors	Average Three-Sigma Values	Test RMSE
Model 0	1	{IC PH 1} (commonly used in the literature)	23	3.88% SOH	1.29% SOH
Model 1	1	{IC PA 1} (selected by the proposed algorithm)	5	1.90% SOH	0.65% SOH
Model 2	2	{IC PA 1, IC PA 2}	7	1.56% SOH	0.53% SOH
Model 3	3	{IC PA 1, IC PA 2, IC PH 1}	10	1.51% SOH	0.52% SOH
Model 4	4	{IC PA 1, IC PA 2, IC PH 1, DV VL 1}	13	1.49% SOH	0.51% SOH
Model 5	5	{IC PA 1, IC PA 2, IC PH 1, DV VL 1, IC PL 1}	23	1.42% SOH	0.48% SOH

The proposed RVR-based SOH estimation model is sparse, namely, a small number of relevance vectors and one offset scalar need to be stored onboard. Only Equations (29) and (30) need to be implemented onboard. These two equations involve low-dimensional matrix multiplications. Take the NMC622 modules as an example. Based on Section VII-A, if one uses two features to estimate SOH, seven 2-by-1 relevance vectors and one offset scalar will be stored onboard and used for all 96 modules. Then, for each module, Equations (29) and (30) involve matrix multiplications among four 8-by-1 vectors and one 8-by-8 matrix.

In summary, the onboard computational footprint of the proposed method in Fig. 2 is small and involves only extracting feature values and performing low-dimensional matrix multiplications. All the computationally intensive optimization and training processes are done offboard. Moreover, SOH monitoring does not need to be performed continuously. Thus, its implementation will not impose special onboard computational requirements.

VIII. CONCLUSIONS

This paper proposes a novel method and demonstrates the feasibility of estimating module-level SOH with high accuracy and confidence in the presence of cell-to-cell variations. First, an information theory-based feature selection algorithm is proposed to find an optimal set of features for SOH estimation under cell-to-cell variations by optimizing feature relevance, redundancy, and complementarity. The optimal feature set found is independent of subsequent learning algorithms. Second, a relevance vector regression (RVR)-based SOH estimation model is proposed. Model sparsity, high estimation accuracy, and good estimation confidence are demonstrated. Applied to a large dataset, the proposed algorithm achieves module-level SOH estimation with 0.53% RMSE and 1.56% average three-sigma value when only two features are used. With more ranked features used in the estimation model, the accuracy can be improved to 0.48% RMSE and 1.42% average three-sigma value. Thus, compared to the estimation results (1.3% RMSE and 3.9% average three-sigma value) obtained by directly applying IC peak-based methods originally developed for the cell level, the proposed method provides significant improvements in estimation performance. As the optimization and training processes are performed offboard, the developed SOH model

can be implemented for onboard execution with low memory and computational requirements.

Results in Sections VI and VII indicate that the same proposed method in Fig. 2 has good generalizability to work well for both cell-level and module-level SOH estimation problems. Different optimal sets of features will be found by the proposed method for cell-level and module-level SOH estimation problems to give good estimation performance.

Future work on the following topics will be pursued to extend and generalize the results reported in this paper. First, making the feature selection algorithm more robust under different operating conditions will be investigated. For example, two experimental datasets used in Sections VI and VII verify the proposed method in a situation where all the originally available features will not disappear throughout the entire degradation process. Future research could be conducted to see how the proposed method performs when some originally available features disappear at some degradation status. Second, how to extend the proposed method to different charging ranges, especially those that do not contain features recommended by the feature selection algorithm, can be investigated in the future. Third, the effects of measurement noise, data acquisition systems, and vehicle chronometrics on the proposed method will be investigated. Fourth, different approaches to estimating cell-to-cell variations within the module, given only module-level measurements, will be explored. Fifth, whether the proposed framework could be applied to estimate the internal resistances of cells and modules for battery power-related performance could also be investigated in the future.

REFERENCES

- [1] A. Barre, B. Deguilhem, S. Grolleau, M. Gerard, F. Suard, and D. Riu, "A review on lithium-ion battery ageing mechanisms and estimations for automotive applications," *Journal of Power Sources*, vol. 241, pp. 680–689, 2013.
- [2] N. Noura, L. Boulon, and S. Jemeï, "A review of battery state of health estimation methods: Hybrid electric vehicle challenges," *World Electric Vehicle Journal*, vol. 11, no. 4, p. 66, 2020.
- [3] M. Bercibar, I. Gandiaga, I. Villarreal, N. Omar, J. V. Mierlo, and P. den Bossche, "Critical review of state of health estimation methods of li-ion batteries for real applications," *Renewable and Sustainable Energy Reviews*, vol. 56, pp. 572–587, 2016.
- [4] "Data standardization requirements for 2026 and subsequent model year light-duty zero emission vehicles and plug-in hybrid electric vehicles," California Code of Regulations, title. 13 § 1962.5.
- [5] L. Yao, S. Xu, A. Tang, F. Zhou, J. Hou, Y. Xiao, and Z. Fu, "A review of lithium-ion battery state of health estimation and prediction methods," *World Electric Vehicle Journal*, vol. 12, no. 3, p. 113, 2021.

- [6] G. L. Plett, "Extended kalman filtering for battery management systems of lipb-based hev battery packs: Part 3. state and parameter estimation," *Journal of Power Sources*, vol. 134, no. 2, pp. 277–292, 2004.
- [7] G. L. Plett, "Sigma-point kalman filtering for battery management systems of lipb-based hev battery packs: Part 2: Simultaneous state and parameter estimation," *Journal of Power Sources*, vol. 161, no. 2, pp. 1369–1384, 2006.
- [8] S. Schwunk, N. Armbruster, S. Straub, J. Keh, and Matthias Vetter, "Particle filter for state of charge and state of health estimation for lithium-iron phosphate batteries," *Journal of Power Sources*, vol. 239, pp. 705–710, 2013.
- [9] I. S. Kim, "A technique for estimating the state of health of lithium batteries through a dual-sliding-mode observer," *IEEE Transactions on Power Electronics*, vol. 25, no. 4, pp. 1013–1022, 2010.
- [10] G. L. Plett, "Recursive approximate weighted total least squares estimation of battery cell total capacity," *Journal of Power Sources*, vol. 196, no. 4, pp. 2319–2331, 2011.
- [11] N. Yang, Z. Song, H. Hofmann, and J. Sun, "Robust state of health estimation of lithium-ion batteries using convolutional neural network and random forest," *Journal of Energy Storage*, vol. 48, p. 103857, 2022.
- [12] H. Chaoui and C. C. Ibe-Ekeocha, "State of charge and state of health estimation for lithium batteries using recurrent neural networks," *IEEE Transactions on Vehicular Technology*, vol. 66, no. 10, pp. 8773–8783, 2017.
- [13] J. Gao, D. Yang, S. Wang, Z. Li, L. Wang, and K. Wang, "State of health estimation of lithium-ion batteries based on mixers-bidirectional temporal convolutional neural network," *Journal of Energy Storage*, vol. 73, no. D, p. 109248, 2023.
- [14] C. Weng, Y. Cui, J. Sun, and H. Peng, "On-board state of health monitoring of lithium-ion batteries using incremental capacity analysis with support vector regression," *Journal of Power Sources*, vol. 235, pp. 36–44, 2013.
- [15] C. Weng, J. Sun, and H. Peng, "Model parametrization and adaptation based on the invariance of support vectors with applications to battery state-of-health monitoring," *IEEE Transactions on Vehicular Technology*, vol. 64, no. 9, pp. 3908–3917, 2015.
- [16] C. Weng, J. Sun, and H. Peng, "A unified open-circuit-voltage model of lithium-ion batteries for state-of-charge estimation and state-of-health monitoring," *Journal of Power Sources*, vol. 258, no. 9, pp. 228–237, 2014.
- [17] M. Dubarry, V. Svoboda, R. Hwu, and B. Y. Liaw, "Incremental capacity analysis and close-to-equilibrium ocv measurements to quantify capacity fade in commercial rechargeable lithium batteries," *Electrochemical and Solid-State Letters*, vol. 9, no. 10, p. A454, 2006.
- [18] A. Krupp, E. Ferg, F. Schuldt, K. Derendorf, and C. Agert, "Incremental capacity analysis as a state of health estimation method for lithium-ion battery modules with series-connected cells," *Batteries*, vol. 7, no. 1, p. 2, 2021.
- [19] Q. Zhou, E. Hellström, D. Anderson, and J. Sun, "Sensitivity analysis of support vector regression-based incremental capacity analysis for battery state of health estimations," in *2023 IEEE Conference on Control Technology and Applications (CCTA)*, Bridgetown, Barbados, 2023, pp. 1122–1127.
- [20] L. Wang, C. Pan, L. Liu, Y. Cheng, and X. Zhao, "On-board state of health estimation of lifepo4 battery pack through differential voltage analysis," *Applied Energy*, vol. 168, pp. 465–472, 2016.
- [21] G. L. Plett, *Battery Management Systems, Volume II: Equivalent-Circuit Methods*. Boston, MA: Artech House, 2015.
- [22] X. Gong, R. Xiong, and C. C. Mi, "Study of the characteristics of battery packs in electric vehicles with parallel-connected lithium-ion battery cells," *IEEE Transactions on Industry Applications*, vol. 51, no. 2, pp. 1872–1879, 2015.
- [23] M. Baumann, L. Wildfeuer, S. Rohr, and M. Lienkamp, "Parameter variations within li-ion battery packs – theoretical investigations and experimental quantification," *Journal of Energy Storage*, vol. 18, pp. 295–307, 2018.
- [24] M. Brand, D. Quinger, G. Walder, A. Jossen, and M. Lienkamp, "Ageing inhomogeneity of long-term used bev-batteries and their reusability for 2nd-life applications," in *AElectric Vehicle Symposium and Exhibition (EVS 26)*, Los Angeles, US, 2012, p. 1–7.
- [25] C. Pastor-Fernández, T. Bruen, W. Widanage, M. Gama-Valdez, and J. Marco, "A study of cell-to-cell interactions and degradation in parallel strings: implications for the battery management system," *Journal of Power Sources*, vol. 329, p. 574–585, 2016.
- [26] F. An, J. Huang, C. Wang, Z. Li, J. Zhang, S. Wang, and P. Li, "Cell sorting for parallel lithium-ion battery systems: Evaluation based on an electric circuit model," *Journal of Energy Storage*, vol. 6, pp. 195–203, 2016.
- [27] C. Weng, X. Feng, J. Sun, and H. Peng, "State-of-health monitoring of lithium-ion battery modules and packs via incremental capacity peak tracking," *Applied Energy*, vol. 180, pp. 360–368, 2016.
- [28] L. Wang, X. Zhao, L. Liu, and C. Pan, "State of health estimation of battery modules via differential voltage analysis with local data symmetry method," *Electrochimica Acta*, vol. 256, pp. 81–89, 2017.
- [29] D. Anseán, V. M. García, M. González, C. Blanco-Viejo, J. C. Viera, Y. F. Pulido, and L. Sánchez, "Lithium-ion battery degradation indicators via incremental capacity analysis," *IEEE Transactions on Industry Applications*, vol. 55, no. 3, pp. 2992–3002, 2019.
- [30] R. Zhou, R. Zhu, C.-G. Huang, and W. Peng, "State of health estimation for fast-charging lithium-ion battery based on incremental capacity analysis," *Journal of Energy Storage*, vol. 51, p. 104560, 2022.
- [31] I. Bloom, A. N. Jansen, D. P. Abraham, J. Knuth, S. A. Jones, V. S. Battaglia, and G. L. Henriksen, "Differential voltage analyses of high-power, lithium-ion cells: 1. technique and application," *Journal of Power Sources*, vol. 139, no. 1-2, pp. 295–303, 2005.
- [32] J. Li, K. Cheng, S. Wang, F. Morstatter, R. P. Trevino, J. Tang, and H. Liu, "Feature selection: A data perspective," *ACM Computing Surveys*, vol. 50, no. 6, p. 1–45, 2017.
- [33] W. Gao, S. Kannan, S. Oh, and P. Viswanath, "Estimating mutual information for discrete-continuous mixtures," in *Advances in Neural Information Processing Systems 30 (NIPS 2017)*, Long Beach, US, 2017, p. 5988–5999.
- [34] O. C. Mesner and C. R. Shalizi, "Conditional mutual information estimation for mixed, discrete and continuous data," *IEEE Transactions on Information Theory*, vol. 67, no. 1, pp. 464–484, 2021.
- [35] T. M. Cover and J. A. Thomas, *Elements of Information Theory*. Hoboken, US: Wiley, 2006.
- [36] A. Kraskov, H. Stögbauer, and P. Grassberger, "Estimating mutual information," *Physical Review E*, vol. 69, p. 066138, 2004.
- [37] P. A. Estevez, M. Tesmer, C. A. Perez, and J. M. Zurada, "Normalized mutual information feature selection," *IEEE Transactions on Neural Networks*, vol. 20, no. 2, pp. 189–201, 2009.
- [38] T. O. Kvålseth, "On normalized mutual information: Measure derivations and properties," *Entropy*, vol. 19, no. 11, p. 631, 2017.
- [39] F. Ferri, P. Pudil, M. Hatef, and J. Kittler, "Comparative study of techniques for large-scale feature selection," *Machine Intelligence and Pattern Recognition*, vol. 16, pp. 403–413, 1994.
- [40] G. Brown, A. Pocock, M.-J. Zhao, and M. Lujan, "Conditional likelihood maximisation: a unifying framework for information theoretic feature selection," *Journal of Machine Learning Research*, vol. 13, pp. 27–66, 2012.
- [41] J. R. Vergara and P. A. Estévez, "A review of feature selection methods based on mutual information," *Neural Computing and Applications*, vol. 24, p. 175–186, 2014.
- [42] J. Runge, "Conditional independence testing based on a nearest-neighbor estimator of conditional mutual information," in *Proceedings of the Twenty-First International Conference on Artificial Intelligence and Statistics, PMLR*, Playa Blanca, Canary Islands, 2018, pp. 938–947.
- [43] M. E. Tipping, "Bayesian inference: An introduction to principles and practice in machine learning," *Advanced Lectures on Machine Learning*, vol. 3176, p. 41–62, 2003.
- [44] D. J. C. MacKay, "Bayesian interpolation," *Neural Computation*, vol. 4, no. 3, p. 415–447, 1992.
- [45] M. E. Tipping, "The relevance vector machine," in *Advances in Neural Information Processing Systems 12 (NIPS 1999)*, Denver, US, 1999, pp. 652–658.
- [46] M. E. Tipping, "Sparse bayesian learning and the relevance vector machine," *Journal of Machine Learning Research*, vol. 1, pp. 211–244, 2001.
- [47] C. Robert, *The Bayesian Choice: From Decision-Theoretic Foundations to Computational Implementation*. Berlin, Germany: Springer Science and Business Media, 2007.
- [48] F. Steinke, M. Seeger, and K. Tsuda, "Experimental design for efficient identification of gene regulatory networks using sparse bayesian models," *BMC Systems Biology*, vol. 1, p. 51, 2007.

- [49] R. M. Neal, *Bayesian Learning for Neural Networks*. Berlin, Germany: Springer Science and Business Media, 1996.
- [50] C. Birkel, "Diagnosis and prognosis of degradation in lithium-ion batteries," Ph.D. dissertation, University of Oxford, Oxford, United Kingdom, May 2017.
- [51] "Oxford dataset," 2017. [Online]. Available: <https://ora.ox.ac.uk/objects/uuid:7d8ccb9c-1469-4209-9995-5871fc908b54>
- [52] X. Tang, Y. Wang, Q. Liu, and F. Gao, "Reconstruction of the incremental capacity trajectories from current-varying profiles for lithium-ion batteries," *iScience*, vol. 24, p. 103103, 2021.
- [53] J. L. Hodges, "The significance probability of the smirnov two-sample test," *Arkiv för matematik*, vol. 3, no. 43, pp. 469–486, 1958.
- [54] F. W. Scholz and M. A. Stephens, "K-sample anderson–darling tests," *Journal of the American Statistical Association*, vol. 82, no. 399, pp. 918–924, 1987.
- [55] T. W. Anderson, "On the distribution of the two-sample cramér-von mises criterion," *The Annals of Mathematical Statistics*, vol. 33, no. 3, pp. 1148–1159, 1962.